Atomic data for non-thermal electron excitation of coronal ions: application to FeXIII

Jacques Dubau

Introduction:

In solar corona modellings, it is usually assumed free electrons to be Maxwellian, corresponding to some temperature T_e. To simulate dynamic phenomenae, a refinement is to introduce a high energy tail (or a Kappa-distribution) : indeed, fast electrons are more difficult to thermalize than low energy electrons... Unfortunately, the effect of high-energy electrons is often smeared by the low energy electron contribution, because cross-section decreases with energy. But, we saw yesterday, that for a line ratio done between 2 lines issued from 2 levels of different excitation energy, the high energy tail can play an important role... Non-thermal ? but what's about the free electron angular distribution: isotropic or anisotropic ?

Electron distribution is assumed axial symmetric around the quantization axis (z) used to define atomic sublevels $|\alpha J M_J\rangle$. It can be developed on Legendre polymonials: $(P_0(cos\Theta) = 1,\ P_2(cos\Theta) = \frac{1}{2}(3(cos\Theta)^2 - 1), ...)$

$$g(v,\Theta) = \sum_{K=0}^{\infty} g_K(v)\, P_K(cos\Theta) \qquad (1)$$

$$\text{where :} \quad \int_0^{\infty} dv \int_0^{\pi} d\Theta\, g(v,\Theta)\, v^2\, sin\Theta = 1 \qquad (2)$$

$$g_K(v) = \frac{2K+1}{2} \int_0^{\pi} P_K(cos\Theta)\, g(v,\Theta)\, sin\Theta\, d\Theta \qquad (3)$$

e.g. $g_K(v) = \frac{1}{2}(2K+1)\,\delta(v - v_0)$ **for an electron beam**

$(v = v_0,\ \Theta = 0) \Rightarrow g(v,\Theta) = \delta(v - v_0)\,\delta(\Theta)/sin\Theta$

Table I. FeXIII energy levels from NIST Tables ($1s^2\ 2s^2\ 2p^6$)

Index	α		J	Energy (Ryd = 13.606 eV)
1	$3s^2\ 3p^2$	^{3}P	0	0.0000
2	$3s^2\ 3p^2$	^{3}P	1	0.0848
3	$3s^2\ 3p^2$	^{3}P	2	0.1691
4	$3s^2\ 3p^2$	^{1}D	2	0.4380
5	$3s^2\ 3p^2$	^{1}S	0	0.8339
20	$3s^2\ 3p\ 3d$	^{3}P	1	4.5102
24	$3s^2\ 3p\ 3d$	^{3}D	2	4.6406
25	$3s^2\ 3p\ 3d$	^{3}D	3	4.6400
26	$3s^2\ 3p\ 3d$	^{1}F	3	5.0745

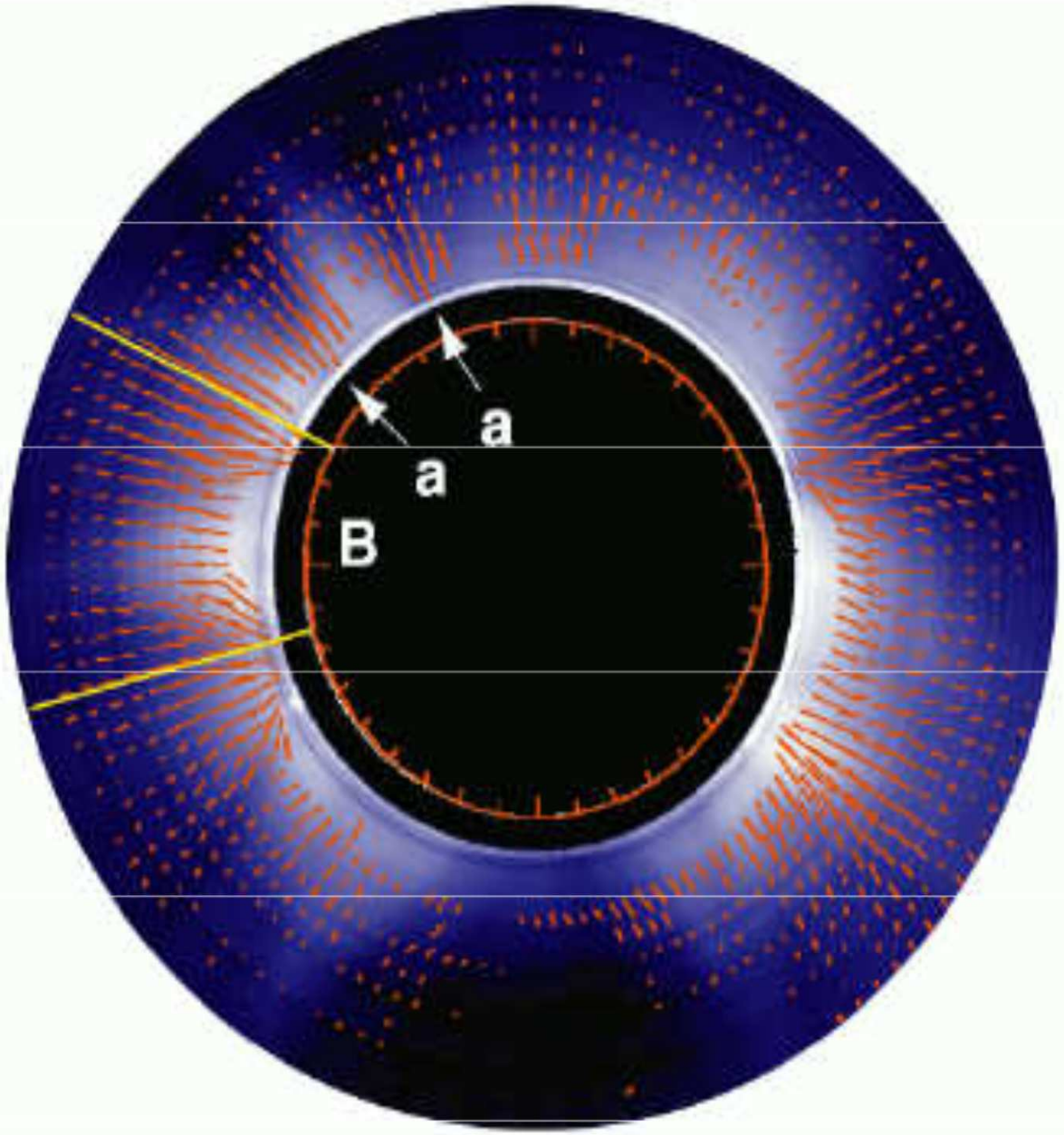

Fig. 3. February 23, 1980 KELP polarization map of the 1074.7 nm FeXIII line superimposed on a Mauna Loa K-corona image obtained the same day (from Habbal *et al.* 2001).

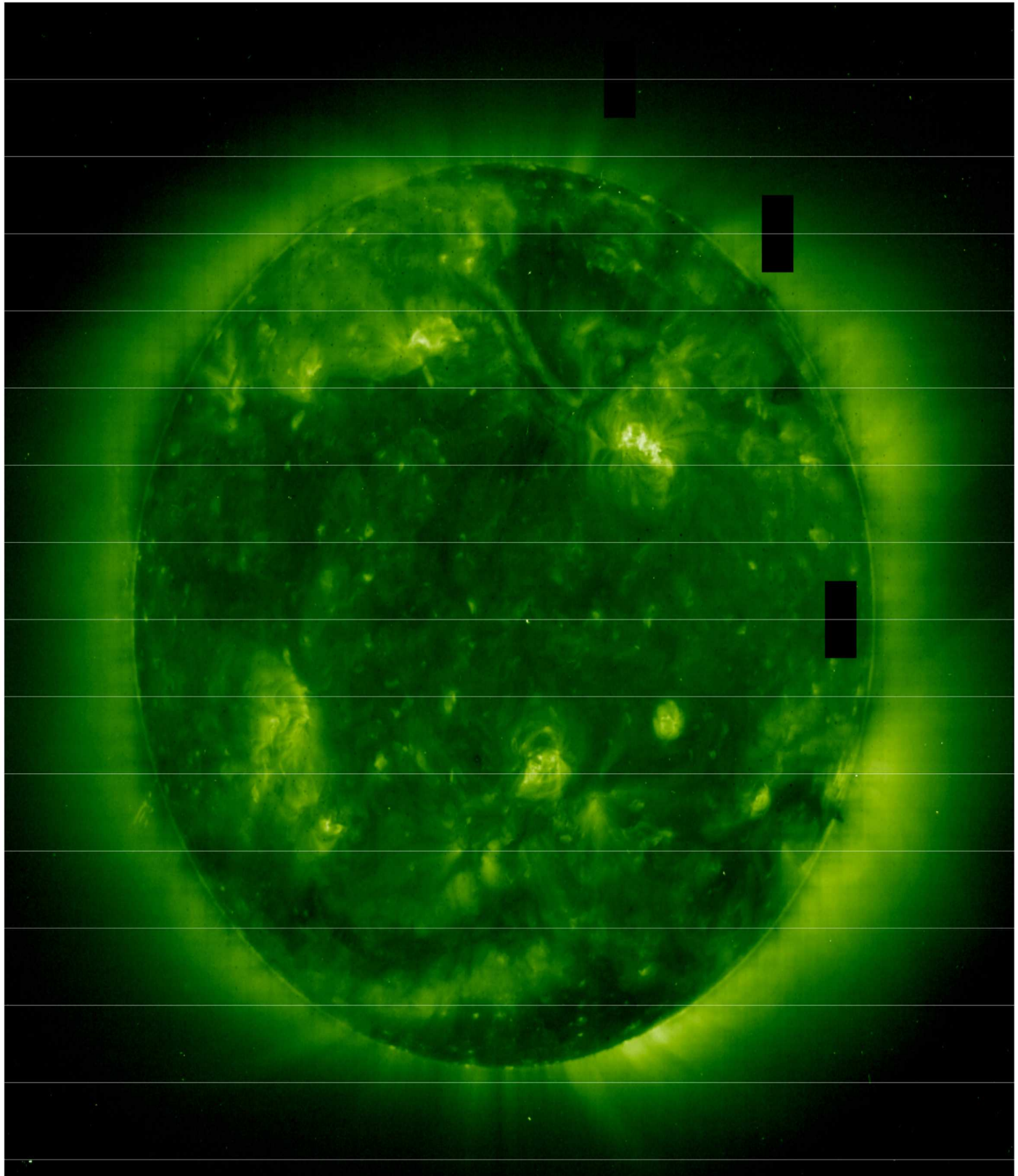

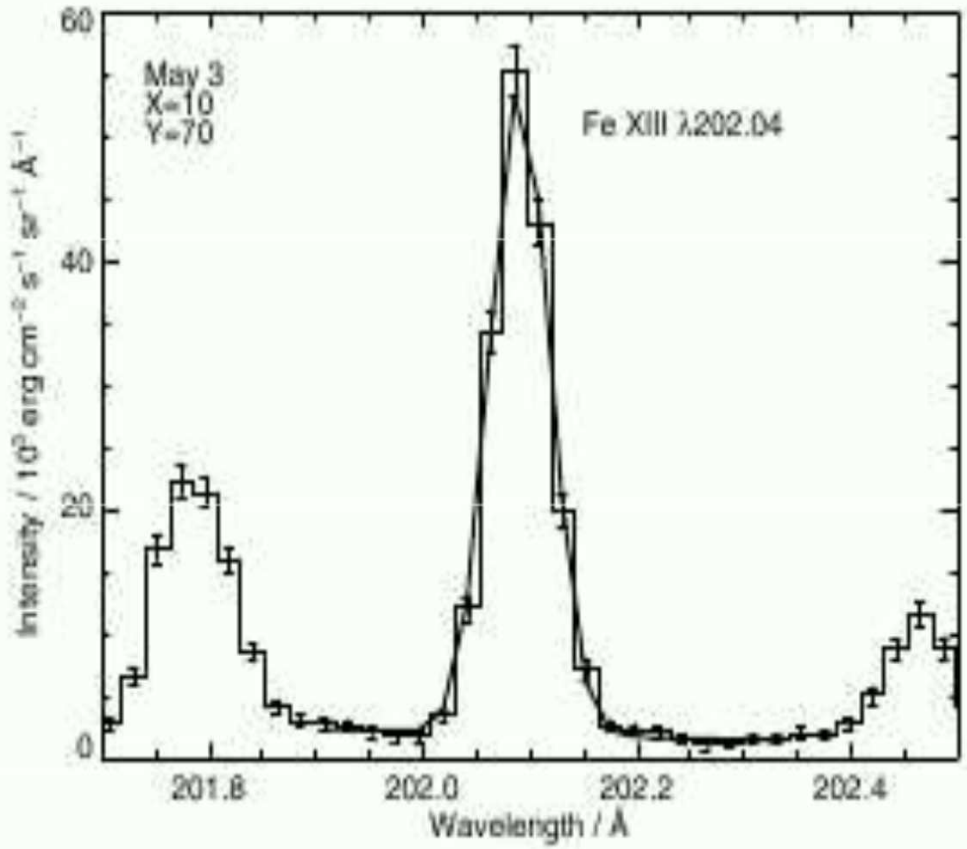

Fig. 8. An example single Gaussian fit to the Fe XIII λ202.0 emission line. The May 3 data set is used, and the image pixel indicated.

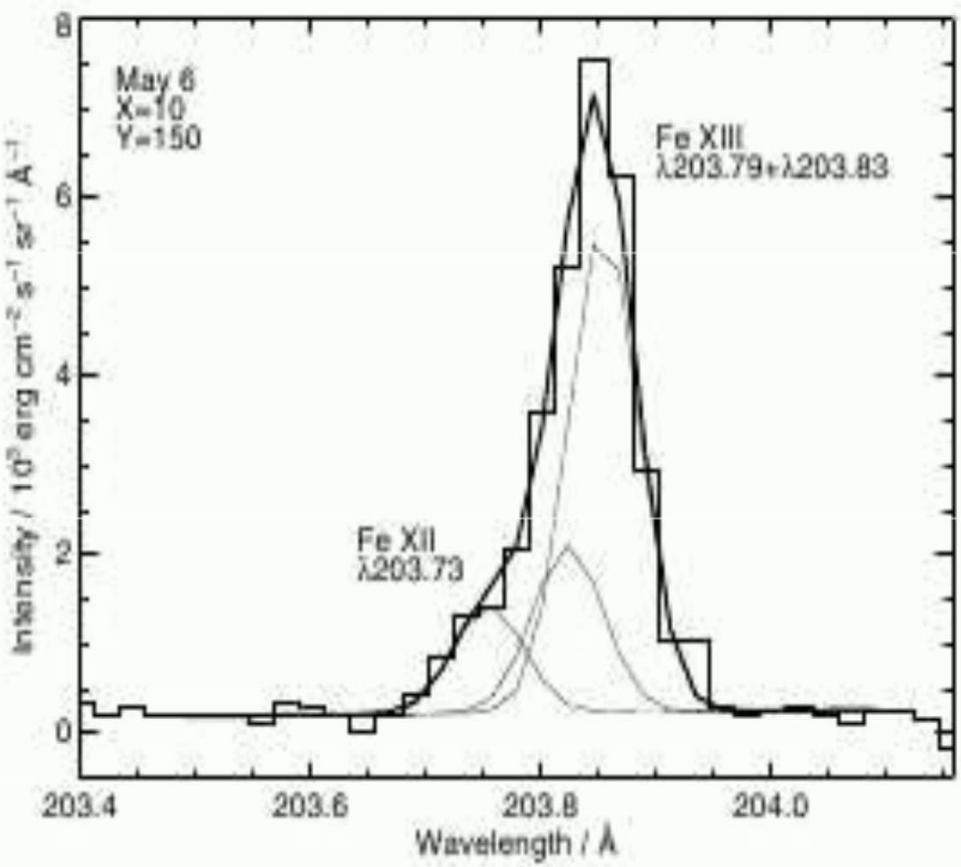

Fig. 9. An example fit to the feature at 203.8 Å that comprises Fe XII λ203.72, and Fe XIII $\lambda\lambda$203.79, 203.83 from the May 6 data set. The spatial pixel chosen is indicated. Three thin lines are used to show the three individual Gaussians from the fit.

Intensity ratio as function of Θ $(\alpha_i J_i \rightarrow \alpha_f J_f)$:

$$I(\text{anisotropic: } \eta \neq 0)/I(\text{isotropic : } \eta = 0)$$

$$-0.5 \leq \eta \leq +0.25$$

$$\frac{I(\eta,\Theta)}{I(\eta=0)} = 1 + (3\cos^2\Theta - 1)\eta, \qquad \eta = W(\alpha_i J_i\, \alpha_f J_f)\,\frac{\rho^2_0(\alpha_i J_i)}{\rho^0_0(\alpha_i J_i)}$$

$$\text{where} \quad W(\alpha_i J_i\, \alpha_f J_f) = \frac{1}{2\sqrt{2}}\,\frac{\begin{Bmatrix} J_i & J_i & 2 \\ 1 & 1 & J_f \end{Bmatrix}}{\begin{Bmatrix} J_i & J_i & 0 \\ 1 & 1 & J_f \end{Bmatrix}} \qquad (\mathrm{M1},\mathrm{E1})$$

- **Level population** $N(\alpha_i J_i) = \rho^0_0(\alpha_i J_i)\sqrt{2J_i+1}$,
- **Level alignment** $\rho^2_0(\alpha_i J_i)$

(see Sahal-Bréchot S. 1977, Ap. J, 213, 887)

$$J_i = 0 : \ \frac{\rho_0^2(\alpha_i J_i)}{\rho_0^0(\alpha_i J_i)} = 0;$$

$$J_i = 1 : \ \frac{\rho_0^2(\alpha_i J_i)}{\rho_0^0(\alpha_i J_i)} = \frac{\sqrt{2}\,(N_1 - N_0)}{N(\alpha_i J_i)};$$

$$J_i = 2 : \ \frac{\rho_0^2(\alpha_i J_i)}{\rho_0^0(\alpha_i J_i)} = \sqrt{\frac{10}{7}}\,\frac{(2N_2 - N_1 - N_0)}{N(\alpha_i J_i)}; \quad \text{etc.}$$

(N_i is the population of the sublevel $|M_{J_i}|$)

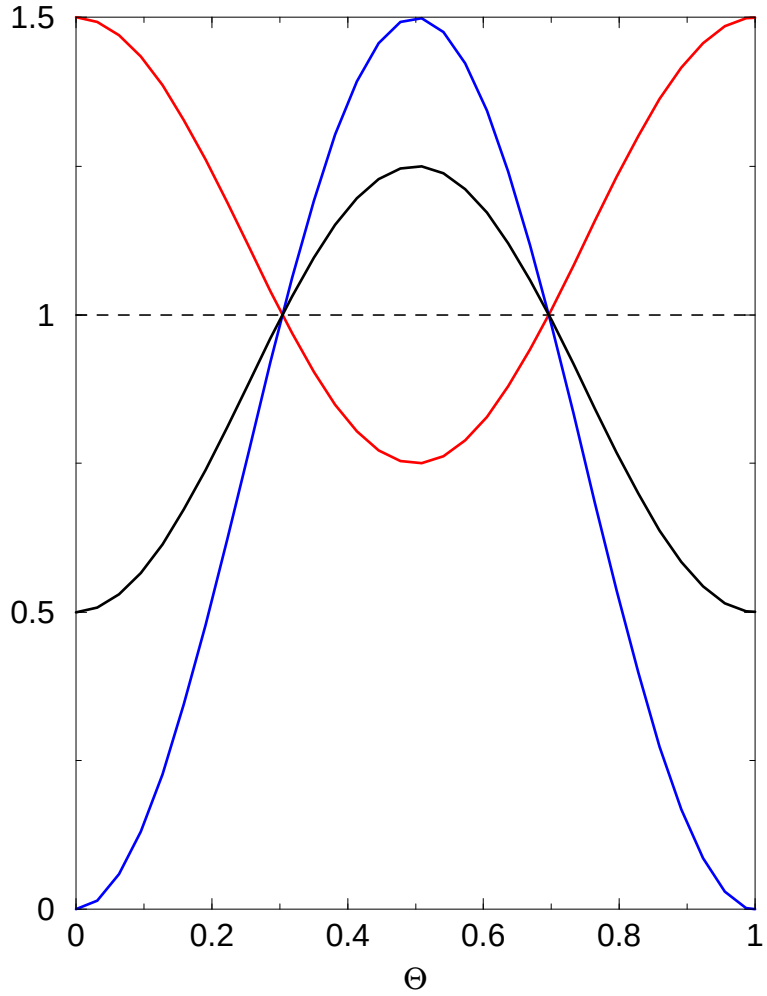

Figure 1: $I(\eta, \Theta)/I(\eta = 0)$: $\eta = -0.50$, $\eta = -0.25$, $\eta = +0.25$

Table 2. Fe XIII wavelengths and $W(\alpha_i J_i\, \alpha_f J_f)$ "algebraic" coefficients

Wavelength (Å)	i - f	J_i - J_f	$W(\alpha_i J_i\, \alpha_f J_f)$
10747 (IR)	2 - 1	1 - 0	+ 0.3536
10798 (IR)	3 - 2	2 - 1	+ 0.2092
196.540 (UV)	26 - 4	3 - 2	+ 0.1732
202.044 (UV)	20 - 1	1 - 0	+ 0.3536
203.797 (UV)	24 - 3	2 - 2	− 0.2092
203.828 (UV)	25 - 3	3 - 2	+ 0.1732

Table 3. Percentage occupation numbers for FeXIII
(Young, Mason and Thomas, Proc. 3rd SOHO Workshop)

Level	10^8	10^9	10^{10}	10^{11}	(cm^{-3})
$(3s^2 3p^2)\,{}^3P_0$	88	41	14	8.9	
${}^3P_1$	6.9	27	30	25	
${}^3P_2$	5.5	30	45	38	
${}^1D_2$	0.07	1.4	11	23	
${}^1S_0$	0.001	0.01	0.2	1.5	

Table 4.1 Collision strength for $K = 2$ angular distribution, E = 15 Ryd (204 eV), $\rho_0^2(i) \leftarrow \rho_0^0(j)$

i	j	$\Omega^2_{2,0}$	i	j	$\Omega^2_{2,0}$
2	1	- 6.250-4	25	1	- 3.822-5
3	1	+1.783-3	25	2	- 1.305-4
3	2	+1.142-3	25	3	- 3.273-2
20	1	- 6.604-2	26	1	- 1.374-4
20	2	- 2.108-4	26	2	- 2.719-4
20	3	- 1.759-3	26	3	- 1.329-3
24	1	- 5.549-5			
24	2	- 1.563-2			
24	3	+1.863-2			

Collision strengths, for $K = 0$ angular distribution, $\Omega^0_{0,0}$, $\rho^0_0(\alpha_i J_i) \leftarrow \rho^0_0(\alpha_j J_j)$. They are related to usual collision strengths $\Omega_{i\,j}$, which are symmetric, i.e. $\Omega_{i\,j} = \Omega_{j\,i}$:

$$\Omega^0_{0,0}(i\,j) = \sqrt{\frac{2J_i + 1}{2J_j + 1}}\,\Omega_{i\,j}$$

Assuming a coronal model (excitation $j \rightarrow i$, radiation $i \rightarrow f$) and an electron beam distribution, we have:

$$\frac{\rho^2_0(i)}{\rho^0_0(i)} = \frac{g_2(v)\,\Omega^2_{2,0}(i\,j)}{g_0(v)\,\Omega^0_{0,0}(i\,j)} = \frac{5\,\Omega^2_{2,0}(i\,j)}{\Omega^0_{0,0}(i\,j)}$$

Table 5.1 Collision strengths Ω_{ji}, compared to AK [3], FM[4]
E=15 Ryd. $(a\text{-}b \equiv a \times 10^{-b})$

j	i	present	AK	FM	j	i	present	AK	FM
1	2	2.054-2	2.099-2	2.05-2	1	25	6.989-3	8.073-3	6.80-3
1	3	9.933-2	9.349-2	9.80-2	2	25	2.180-2	2.589-2	2.18-2
2	3	2.259-1	2.178-1	2.08-1	3	25	6.404-0	6.063-0	8.48-0
1	20	1.710-0	1.622-0	2.71-0	1	26	3.534-3	3.915-3	3.60-3
2	20	6.592-3	9.454-3	1.37-1	2	26	1.187-2	1.311-2	1.25-2
3	20	4.470-1	3.888-1	2.68-1	3	26	1.807-1	2.170-1	3.38-1
1	24	1.920-3	2.599-3	1.40-3					
2	24	1.484-0	1.379-0	1.51-0					
3	24	2.076-0	1.949-0	3.25-0					

Table 6. $\frac{\rho_0^2(i\,j)}{\rho_0^0(i\,j)}$ and $\eta(i\,f)$ for E = 15, 30, 45 Ryd.

j	i	f	$\frac{\rho_0^2}{\rho_0^2}(15)$	$\eta(15)$	$\frac{\rho_0^2}{\rho_0^2}(30)$	$\eta(30)$	$\frac{\rho_0^2}{\rho_0^2}(45)$	$\eta(45)$
1	20	1	− 0.115	− 0.041	− 0.060	− 0.021	− 0.022	− 0.008
2	24	3	− 0.040	+ 0.008	− 0.022	+ 0.005	− 0.008	+ 0.002
3	24	3	+ 0.045	− 0.009	+ 0.028	− 0.006	+ 0.015	− 0.003
3	25	3	− 0.022	− 0.004	− 0.010	− 0.002	− 0.001	− 0.000

For the first line ($j = f = 1$, $i = 20$), at $E = 5.5$ Ryd

$$\frac{\rho_0^2}{\rho_0^2}(5.5) = -0.131 \text{ and } \eta(5.5) = -0.046$$

References

- [1] Arnaud, J. 2003, EAS Publication Series 9, 209
- [2] Young, P.R., Watanabe, T., Hara, H. & Mariska, J.T. 2009, A & A 495, 587
- [3] Aggarwal, K.M. & Keenan F.P. 2004, A & A 418, 371
- [4] Fawcett, B. C. & Mason, H.E. 1989, ADNDT 43, 245

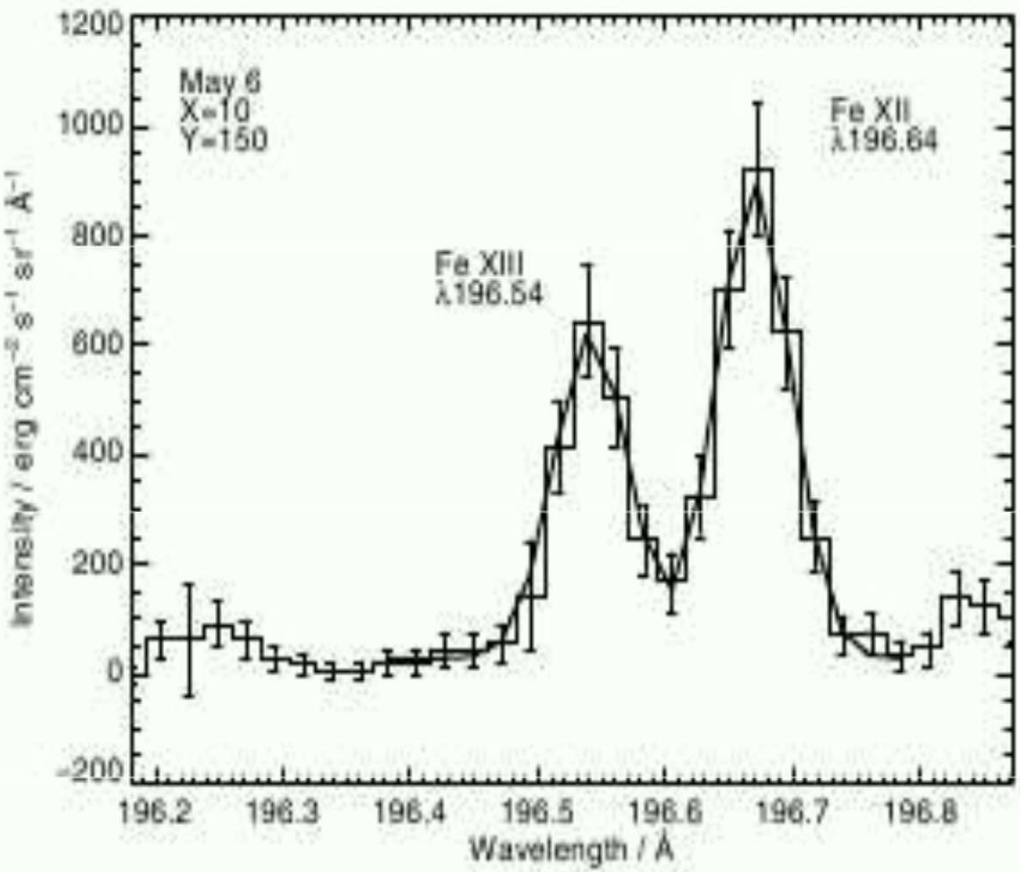

Fig. 7. An example double-Gaussian fit to Fe XIII λ196.54 and Fe XII λ196.64 from the May 6 data set. The chosen spatial pixel is indicated. The data are plotted as a thin line and the fit with a thick line. The error bars on the intensity measurements are also shown.

Table 4.2 Collision strength for $K = 2$ angular distribution, E = 30 Ryd (408 eV)

i	j	$\Omega^2_{2,0}$	i	j	$\Omega^2_{2,0}$
2	1	-3.418-4	25	1	+7.900-5
3	1	+1.724-3	25	2	+4.449-5
3	2	+1.034-3	25	3	-1.584-2
20	1	-3.813-2	26	1	-4.617-5
20	2	-7.234-5	26	2	-9.533-5
20	3	-1.467-3	26	3	-7.224-4
24	1	-1.815-5			
24	2	-8.986-3			
24	3	+1.242-2			

Table 4.3 Collision strength for $K = 2$ angular distribution, E = 45 Ryd (612 eV)

i	j	$\Omega^2_{2,0}$	i	j	$\Omega^2_{2,0}$
2	2	-2.103-4	25	1	+1.403-4
3	1	+1.725-3	25	2	+1.253-4
3	2	+9.964-4	25	2	-1.267-3
20	1	-1.358-2	26	1	-1.627-5
20	2	-2.674-5	26	2	-3.866-5
20	3	-1.226-3	26	3	-2.951-4
24	1	-5.981-6			
24	2	-3.084-3			
24	3	+6.827-3			

Table 5.2 Collision strengths Ω_{ji}, compared to AK [3], FM[4]
E=30 Ryd. $(a\text{-}b \equiv a \times 10^{-b})$

j	i	present	AK	FM	j	i	present	AK	FM
1	2	1.133-2	1.189-2	1.12-2	1	25	6.616-3	7.265-3	5.70-3
1	3	9.888-2	9.320-2	8.42-2	2	25	2.354-2	2.031-2	1.64-2
2	3	2.051-1	2.175-1	1.70-1	3	25	6.842-0	7.274-0	1.00+1
1	20	1.857-0	1.980-0	3.20-0	1	26	1.871-3	2.051-3	1.90-3
2	20	3.340-3	5.408-3	1.58-1	2	26	6.081-3	6.553-3	6.30-3
3	20	4.833-1	4.573-1	3.11-1	3	26	1.849-1	2.457-1	3.86-1
1	24	9.965-4	1.353-3	7.00-4					
2	24	1.603-0	1.644-0	1.79-0					
3	24	2.252-0	2.317-0	3.83-0					

Table 5.3 Collision strengths Ω_{ji}, compared to AK [3], FM[4]
E=45 Ryd. $(a\text{-}b \equiv a \times 10^{-b})$

j	i	present	AK	FM	j	i	present	AK	FM
1	2	7.216-3	7.643-3	7.00-3	1	25	6.662-3	7.131-3	5.00-3
1	3	9.644-2	9.608-2	7.47-2	2	25	1.696-2	1.852-2	1.34-2
2	3	1.952-1	2.390-1	1.47-1	3	25	6.634-0	8.103-0	1.12+1
1	20	1.821-0	2.216-0	3.57-0	1	26	1.187-3	1.310-3	1.20-3
2	20	1.977-3	3.915-3	1.74-1	2	26	3.677-3	3.938-3	3.70-3
3	20	4.746-1	5.122-1	3.44-1	3	26	1.771-1	2.683-1	4.26-1
1	24	6.013-4	8.449-4	4.00-4					
2	24	1.567-0	1.837-0	1.99-0					
3	24	2.211-0	2.594-0	4.27-0					